Evaluation of the Potential of Hyperion for Fire Danger Assessment by Comparison to the Airborne Visible/Infrared Imaging Spectrometer

Dar A. Roberts, *Member, IEEE*, Philip E. Dennison, *Student Member, IEEE*, Margaret E. Gardner, Yasha Hetzel, Susan L. Ustin, *Member, IEEE*, and Christopher T. Lee, *Member, IEEE*

***Abstract*—Parameters derived from remote sensing that can be used to assess fire danger include surface reflectance, live and dead biomass, canopy water content, species composition, and fuel state. Spectral bands and wavelength locations of traditional multispectral data make assessment of fire danger in Mediterranean shrublands difficult, although fire danger parameters have been derived from Airborne Visible/Infrared Imaging Spectrometer (AVIRIS) data. We compare nearly simultaneous acquisition of Hyperion and AVIRIS to evaluate spaceborne monitoring potential of fire danger in Southern California chaparral. Field spectra were acquired to support reflectance retrieval and construct a spectral library for vegetation mapping. Reflectance spectra retrieved from Hyperion and AVIRIS had similar shape and albedo, but SNR was five times higher in AVIRIS. Fuel condition was assessed using the endmember fractions from spectral mixture analysis, with both Hyperion and AVIRIS imaging spectrometer data providing similar fractions and spatial distributions. Hyperion demonstrated good capability for separating spectral signals from bare soil and dry plant litter. Canopy water content was compared using the 980- and 1200-nm liquid water bands, the water index, and the normalized difference water index. Results showed that Hyperion is capable of retrieving canopy water at 1200 nm, but demonstrates poor performance at 980 nm. Sensor noise and instrumental artifacts account for poor performance in this spectral region. Overall, full-spectrum measures outperformed band ratios because of a lower sensitivity to sensor noise in individual bands. Species and community mapping showed similar patterns with better accuracy for AVIRIS relative to Hyperion, but with both instruments achieving only 79% and 50% overall accuracy, respectively.**

***Index Terms*—Airborne Visible/Infrared Imaging Spectrometer (AVIRIS), fuel load, fuel model, fuel moisture, Hyperion, imaging spectrometry, spectral mixture analysis, wildfire.**

Manuscript received June 21, 2002; revised January 22, 2003. This work was supported by the National Aeronautics and Space Administration Earth Observing 1 Science Validation Program under Grant NCC5–496, by the Solid Earth and Natural Hazards Program under Grant NAG2–1140, and by the Regional Earth Science Application Center (RESAC) Program under Grant CSDH NASA RESAC 447633–59075.

D. A. Roberts, P. E. Dennison, M. E. Gardner, and Y. Hetzel are with the Department of Geography, University of California, Santa Barbara, CA 93106 USA (e-mail: dar@geog.ucsb.edu).

S. L. Ustin is with the Department of Air, Land and Water Resources, University of California, Davis, CA 95616 USA.

C. T. Lee is with the Department of Geography, California State University Long Beach, CA 90840 USA.

Digital Object Identifier 10.1109/TGRS.2003.812904

I. Introduction

WILDFIRE is a major global disturbance mechanism, impacting large areas of boreal forests, savannas, Mediterranean ecosystems, and even tropical rainforest [1]–[4]. In Southern California, a Mediterranean climate with hot dry summers results in summer water deficits and ecosystems that are highly sensitive to climate perturbations. Summer drought coupled with the presence of shrub and forested communities along the wildland urban interface make wildfire one of the most serious economic and life-threatening natural disasters in the region [5], with an average annual cost of US $163 million dollars due to home and property loss state wide [6]. Fire return intervals range from less than a decade to over 50 years. The potential of catastrophic wildfire is further exacerbated by extreme weather events (i.e., Santa Ana Winds), more than 70 years of fire suppression [7], and periods of extended drought. Postfire effects, such as erosion and mud slides from fire-burned slopes, often exceed the cost of the original fire in damage [8].

Four fuel characteristics are essential for understanding the behavior of wildfire: fuel type, fuel biomass, fuel moisture, and fuel condition. Fuel type describes species-specific combustion properties including surface-area-to-volume ratio, relative amounts of herbaceous and woody fuels, and phenology. Traditional fuel models for fire behavior modeling have also included typical fuel biomass and fuel condition with fuel type [9]. Fuel biomass describes both live and dead vegetation dry biomass. Biomass of live herbaceous material is particularly important in chaparral, because the structure and chemistry of chaparral leaves make live materials more combustible than in other vegetation types [10]. Fuel moisture is the percentage of liquid water present relative to dry weight in both live and dead fuels. Fuel moisture is potentially the most important fuel property controlling fire hazard [4]. Unlike dead fuel moisture, live fuel moisture does not respond strongly to changes in environmental relative humidity. Finally, fuel condition represents the relative proportion of live to dead (or senesced) fuels. Live fuels contain a higher percentage of liquid water that must be driven off before the fuel undergoes combustion. Dead fuels contain less moisture and react strongly to changes in environmental humidity.

In this paper, we evaluate the potential of Hyperion, an imaging spectrometer on the Earth Observing 1 (EO-1) satellite platform, for wildfire danger assessment. We evaluate Hyperion performance by direct comparison of Hyperion wildfire danger products to Airborne Visible/Infrared Imaging Spectrometer (AVIRIS) products produced from data acquired within two days of the Hyperion overpass. This comparison uses AVIRIS data as the reference dataset. We focus on data acquired in the vicinity of Santa Barbara, CA, in a region dominated by schlerophyllous shrub vegetation typical of Mediterranean climates. This region has experienced a number of catastrophic fires in recent decades, including one of the most destructive in California history, the 1990 Painted Cave Fire [11]. Important remote sensing-based measures that can contribute to fire danger assessment include the following:

1) direct measures of live fuel moisture;
2) measures of live herbaceous biomass;
3) measures of fuel condition;
4) detailed classifications of fuel type.

Accurate and stable retrieved surface reflectance is necessary to produce these measures. To evaluate Hyperion performance, we compared fuel measures derived from a Hyperion scene acquired on June 12, 2001 to similar measures derived from AVIRIS on June 14, 2001. Live herbaceous biomass and fuel moisture were assessed using several hyperspectral measures of canopy moisture. Fuel condition was assessed using green vegetation (GV), nonphotosynthetic vegetation (NPV), and soil as endmembers for spectral mixture analysis (SMA) [12]. Fuel types were mapped using multiple-endmember spectral mixture analysis (MESMA) [13]. MESMA allows endmembers to vary on a per-pixel basis, in contrast to SMA, which uses the same endmembers for the whole scene. Instrument performance and the accuracy of vegetation maps was assessed by comparison with 85 to 91 reference polygons measured in the field.

II. Background

Fire behavior is a product of weather, fuels, and terrain, which vary in importance depending on season and fire regime [4]. Of these factors, fuels are often the most problematic because of their high spatial and temporal variability, resulting in a lack of timely fuels information at an appropriate spatial scale. Fire danger is most often assessed using broadband sensors such as the Advanced Very High Resolution Radiometer, Multispectral Scanner, and Thematic Mapper (TM), through some combination of fuel type mapping, meteorology and ancillary geographic information (such as slope, aspect, and elevation), and fire history [5], [14]–[16]. Most commonly, fuels are mapped using two fuel classification systems; one is described by Anderson [9] and is part of the BEHAVE fire prediction system, and the other is the National Fire Danger Rating System [17].

Roberts *et al.* [18] and Dennison *et al.* [19] describe new measures of fuel properties derived from hyperspectral systems such as AVIRIS. These measures include 1) direct estimates of canopy moisture and live biomass, 2) estimation of fuel condition using SMA, and 3) vegetation mapping at the community and species level using MESMA [18]. Canopy moisture and estimates of green-live biomass can be derived directly from canopy reflectance measured by hyperspectral systems. Examples of moisture indexes include equivalent liquid water thickness (EWT) [20], [21], the normalized difference water index (NDWI) [22], and the water index (WI) [23]. The WI is calculated as the ratio of a wavelength outside the strong 980-nm water band divided by reflectance within this water absorption feature [23]

$$\mathrm{WI} = \frac{\rho_{895}}{\rho_{972}}. \tag{1}$$

NDWI is a normalized difference index the based on wavelengths inside and outside the 1200-nm water absorption feature [22]

$$\mathrm{NDWI} = \frac{(\rho_{857} - \rho_{1241})}{(\rho_{857} + \rho_{1241})}. \tag{2}$$

EWT is estimated from at-sensor radiance or reflectance data using a Beer–Lambert approach in which the spectral expression of liquid water is modeled based on the exponential of the absorption coefficient of liquid water modified by the pathlength within the medium [24].

Ustin *et al.* [25] evaluated the potential of EWT as a measure of canopy moisture in chaparral ecosystems. Serrano *et al.* [26] expanded this analysis to compare the NDWI, EWT, and WI as measures of relative water content (RWC) in chaparral, concluding that WI was most sensitive to RWC, while EWT was more sensitive to canopy structure. These results are consistent with Roberts *et al.* [24], who evaluated the relationship between green leaf area index and EWT, but disagree with [25] and [18], which document seasonal changes in the relationship between measures of canopy greenness and measures of canopy moisture.

SMA can be used to estimate fuel condition, by mapping GV and NPV fractions. The fractions respond to the relative proportions of live (GV) and senesced (NPV) vegetative land cover. Vegetation communities and species can be mapped using MESMA. In MESMA, endmembers are not fixed, but are allowed to vary on a per-pixel basis [13]. The fraction of the dominant cover types is modeled within each pixel. In many cases, it is possible to spectrally distinguish vegetation at the species level. Vegetation maps produced by MESMA can be reclassified to standard fuel models such as those presented by Anderson [9]. Species-level maps can also be used with species-specific fuels information such as surface area-to-volume ratio.

III. Methods

A. Study Site

The study was conducted primarily in the Santa Ynez Mountains, located north of Santa Barbara, CA (34° N, 120° W) in an area of overlapping Hyperion and AVIRIS data acquisitions (Fig. 1). This area is characterized by winter precipitation, summer drought, cool winters, and warm summers. Dominant vegetation in the area is adapted to summer drought, consisting of a variety of schlerophyllous evergreen plants or drought deciduous species. Although a large number of species are present, only a few dominate the landscape including chamise (*Adenostoma fasciculatum*), two species of California lilac (*Ceanothus*

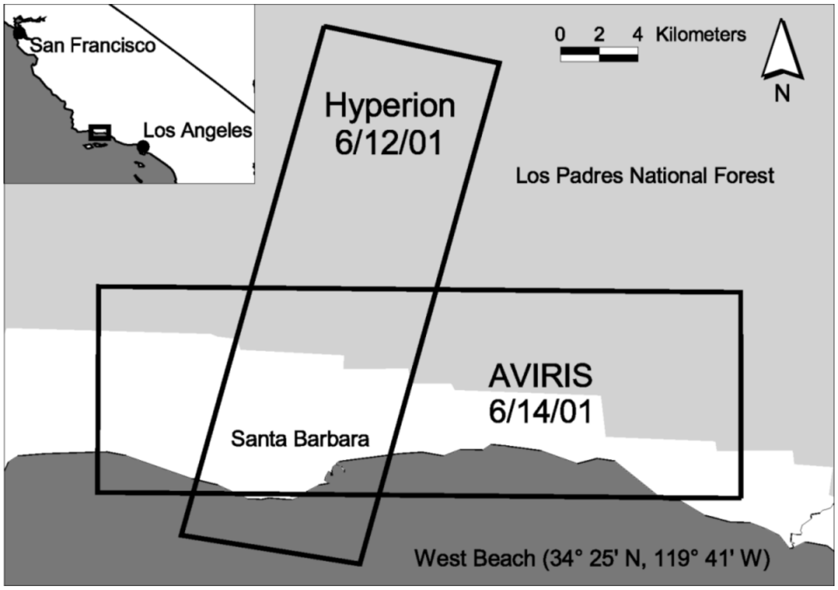

Fig. 1. Index map showing location of study site and areal coverage of Hyperion and AVIRIS.

megacarpus and *C. spinosus*), and two oaks (*Quercus agrifolia* and *Q. dumosa*). Grasslands, which are common at lower elevations on relatively flat terrain, are dominated by a number of European-introduced species. At high elevations, two species of manzanita (*Arctostaphylos glandulosa* and *A. glauca*) are locally abundant. Coastal sage scrub is uncommon on the southern flank of the Santa Ynez Range.

Six land-cover classes were mapped in this study including 1) soil, 2) grassland, 3) chamise, 4) Ceanothus, 5) manzanita, and 6) oak. The two *Ceanothus* species were combined into a single class because with few exceptions *Ceanothus spinosus* rarely occurred in large enough patches to dominate a 20-m pixel. *Quercus dumosa* was not included because this species, while common, was rarely a dominant in any stand.

B. Data

Image data consisted of two remotely sensed datasets, Hyperion acquired at approximately 18:26 UTC (11:26 PDT) on June 12, 2001 and overlapping AVIRIS data acquired at approximately 20:15 UTC (13:15 PDT) on June 14, 2001 (Fig. 1). Hyperion is a spaceborne imaging spectrometer consisting of 242 channels ranging from 356–2577 nm, sampled approximately at a 10-nm sampling interval. It is part of the EO-1 platform and follows Landsat Enhanced TM in its orbit, providing nearly simultaneous coverage. It has a nominal ground instantaneous field of view (GIFOV) of 30 m and 12-bit radiometric quantization. The cross-track swath consists of 256 samples and has a nominal swath width of 7.65 km. Down-track image length can be as high as 185 km, equal to a full Landsat scene (see [27] for details). AVIRIS is an airborne imaging spectrometer that acquires 224 spectral channels between 350–2500 nm at a nominal sampling interval of 10 nm with a GIFOV of 20 m when flown on the ER2 at 20 km height [28]. The typical AVIRIS scene consists of 614 cross-track elements and 512 lines, with a swath width of approximately 12 km. AVIRIS was flown along a roughly east–west flight direction, while Hyperion was acquired along the north–northeast track typical of polar orbiting satellites (Fig. 1). Solar zenith angles were 23° for the Hyperion image acquisition and 12° for the AVIRIS image acquisition. Atmospheric conditions were similar for the two acquisitions, with cloud-free skies over the target area and high visibilities occurring on both dates.

Hyperion data were radiometrically calibrated by TRW using Level 1b processing. Level 1b radiance was corrected using postlaunch calibration equal to a 1.08 multipier applied to radiance for the VNIR and 1.18 multiplier in the SWIR [29]. Noise-equivalent delta radiance (NEdL) was calculated for both AVIRIS and Hyperion from the standard deviation of 100 ocean spectra at 1851 nm, a strong water vapor absorption band. Hyperion and AVIRIS data were geometrically rectified to a 20-m resolution georectified SPOT image, projected to UTM zone 11 using the NAD83 datum.

Field spectra from several homogeneous ground calibration sites were acquired in late May/early June 2001 just prior to the Hyperion acquisition. Spectra were acquired using an Analytical Spectral Devices (ASD) full-range instrument (Analytical Spectral Devices, Boulder, CO). Spectra were measured along transects within 2 h of solar noon ($\pm -30^{\circ}$ solar zenith) and standardized using a Spectralon reference panel (Labsphere, Inc., North Sutton, NH) measured at the start and end of each transect and along the transect at time intervals no greater than 5 min. Transect length was dependent on the size of the target. For this study, a 40-m transect acquired along West Beach was processed to reflectance and averaged (Fig. 1). An area corresponding to the West Beach transect was extracted from Hyperion (six pixels) and AVIRIS (eight pixels) for use in atmospheric correction. ASD spectra were convolved to AVIRIS and Hyperion using bandpass wavelength centers and a Gaussian filter function based on the full-width at half-maximum published for each sensor. The averaged West Beach spectrum was used to remove high-frequency artifacts from both Hyperion and AVIRIS reflectance data, but was not used to produce gross changes in retrieved surface reflectance from each sensor. We use this approach to preserve reflectance differences due to subpixel shadowing.

Over 95 field polygons were identified in the field for use in vegetation mapping and accuracy assessment. Vegetation polygons were field-identified-based on uniform cover and composition and a minimum size criterion of 60 m $\times$ 60 m. For each polygon, species composition was categorized based on percent of total cover: 0% to 10%, 10% to 25%, 25% to 50%, 50% to 75%, 75% to 90%, and 90% to 100%. This approach was selected because 1) chaparral is typically patchy and is rarely dominated by a single species and 2) these broad categories could be quickly identified in the field with high accuracy. Polygons were mapped in the field on 1-m resolution digital orthophoto quads, then digitized in the laboratory and resampled to Hyperion and AVIRIS spatial resolutions. Ultimately, 85 polygons were identified within the Hyperion scene and 91 polygons were identified within the AVIRIS scene, with 79 polygons shared between the two scenes. For accuracy assessment, Hyperion or AVIRIS classifications were considered correct if the dominant species mapped within the polygon agreed with the field estimate of dominance.

C. Image Analysis

1) Reflectance Retrieval: Surface reflectance was retrieved for both datasets using Atmospheric Correction Now ver. 3.12 (ACORN) (Analytical Imaging & Geophysics, Boulder, CO). Hyperion Level 1b radiance was adjusted using postlaunch corrections (1.08 in VNIR, 1.18 in SWIR). To account for spatially varying water vapor, water vapor was estimated using fits performed on both the 940- and 1130-nm regions on both Hyperion and AVIRIS. After an initial reflectance retrieval, Hyperion and AVIRIS reflectance images were adjusted using the West Beach ground target spectra [30].

2) Moisture/Live Biomass: Canopy moisture and live biomass were assessed using four hyperspectral measures, the WI [23], NDWI [22], and EWT [20], [21]. The closest band centers for Hyperion and AVIRIS were used for the numerator and denominator for WI and NDWI. A third band ratio, a modified NDWI (mNDWI), was also calculated. The hyperspectral band closest to the center of the liquid water absorption feature and a reference band in the same focal plane were used to calculate mNDWI for Hyperion

$$\mathrm{mNDWI} = \frac{(\rho_{1070} - \rho_{1200})}{(\rho_{070} + \rho_{1200})}. \tag{3}$$

EWT was estimated from Hyperion and AVIRIS reflectance by regressing the natural logarithm of reflectance against the absorption coefficient of liquid water across two wavelength regions, 865–1088 and 1088–1285 nm [24]. These measures are called EWT980 and EWT1200, respectively.

3) Fuel Condition: Fuel condition is defined here as the proportion of live canopy components to dead canopy components. Fuel condition was mapped using SMA which was used to map green vegetation (green leaves), nonphotosynthetic vegetation (stems, wood, and litter), shade and soil. The reference endmembers used in this study were derived from field and laboratory spectra and are the same as we have used for several years for fuel mapping in the Santa Barbara area and Santa Monica Mountains [18].

4) Fuel Type: Dominant vegetation types were mapped using MESMA [13]. In MESMA, endmember models are selected from the library of potential models based on whether they are physically reasonable (fractions are between 0% and 100%) and meet criteria based on the overall fit (rms) and residuals. Given several models that fit the criteria, the model with the lowest overall rms is selected as the best candidate. Models are evaluated starting with two-endmember combinations between shade and a second material (i.e., GV or NPV from several species and plant communities). For pixels not adequately modeled, the analysis then progresses to more complicated models consisting of three or more endmembers.

Several innovations were employed in this study. First, unlike previous applications [13], in which two-endmember combinations were given precedence over all three-endmember combinations, in this paper two-endmember models were only selected if a three-endmember model provided only slight improvements in fit. The choice between the best two- and three-endmember cases was made if the rms decreased beyond a specified threshold, in this case determined empirically to be 0.008 reflectance (0.8%). A second innovation involved the development of the spectral library. A reference endmember library was constructed from AVIRIS spectra selected from the reference polygons dominated by each vegetation species. In this case, our objective was to develop a library that was parsimonious, including the minimum number of spectra required to map individual species with the least confusion between species. To do this, a spectral library was developed for each species, then analyzed as if it were an image using MESMA, similar to the approach described in [31]. The top three to five spectra for each species were selected starting with the spectrum that met the MESMA criteria for the largest number of spectra within the library, followed by spectra that accounted for the greatest number of spectra that remained unmodeled within the same library. This procedure was repeated for each species we intended to map. Once the best candidates were selected for each species, these spectra were applied to the other spectral libraries, to determine the extent to which they were confused with the wrong species. The value of a spectrum could be determined by a comparison of its ability to map the correct species, compared to confusion with other species. If considerable confusion occurred with only marginal value within it own species, the spectrum was not used as a candidate.

An example is provided for chamise- and oak-dominated endmembers (Table I). For chamise, a library consisting of 92 chamise-dominated spectra was extracted from the AVIRIS image using the reference polygons. MESMA was applied to the chamise-dominated library using the same library as a source, and the spectrum that modeled the greatest number of members of the library was selected as the top candidate. Here, the spectrum evf57.14 modeled 59 out of 92 spectra, accounting for 64.1% of the chamise-dominated library. After selecting this model, MESMA was applied again, but this time excluding evf57.14. The next best spectrum, which accounted for the greatest number of unmodeled chamise spectra in the library, was evf56.5. Ultimately, four chamise-dominated spectra were

TABLE I

MODEL SELECTION AND CONFUSION BETWEEN MODELS. EXAMPLES FOR CHAMISE- AND OAK-DOMINATED ENDMEMBERS ARE SHOWN. SPECTRAL NAMES ARE BASED ON THE REFERENCE POLYGON NAME AND NUMBER OF THE SPECTRUM WITHIN THE POLYGON. THE TOP ROW LISTS THE NUMBER OF SPECTRA WITHIN EACH LIBRARY, EQUAL TO 92 FOR CHAMISE-DOMINATED, 143 FOR CEANOTHUS-DOMINATED (CEANO), 178 FOR OAK-DOMINATED, AND 52 FOR MANZANITA-DOMINATED (MANZA). COLUMNS INCLUDE 1) SPECTRAL NAME, 2) NUMBER MODELED WITHIN THE LIBRARY, 3) PERCENTAGE OF THAT LIBRARY MODELED, 4) PRIORITY OF SELECTION, 5) AND UP, NUMBER MODELED AND PERCENTAGE MODELED OF A DIFFERENT LIBRARY

	N =	92	N =	143	N =	178		52	
Chamise		Percent	Priority	Ceano	Percent	Oak	Percent	Manza	Percent
evf57.14	59	64.1	1	54	37.8	12	6.7	40	76.9
evf56.5	38	41.3	2	8	5.6	4	2.2	25	48.1
evf57.20	38	41.3	3	9	6.3	2	1.1	26	50
evf57.11	31	33.7	4	8	5.6	4	2.2	13	25
	N =	178	N =	92	N =	143		52	
Oak	Oak	Percent	Priority	Chamise	Percent	Ceano	Percent	Manza	Percent
evf86.19	134	75.3	1	2	2.2	60	42	0	0
evf86.16	85	47.8	2	0	0	2	1.4	0	0
evf86.31	55	30.9	3	1	1.1	79	55.2	0	0
evf32.29	41	23	4	5	5.4	95	66.4	0	0
evf32.38	25	14	5	3	3.3	44	30.8	0	0

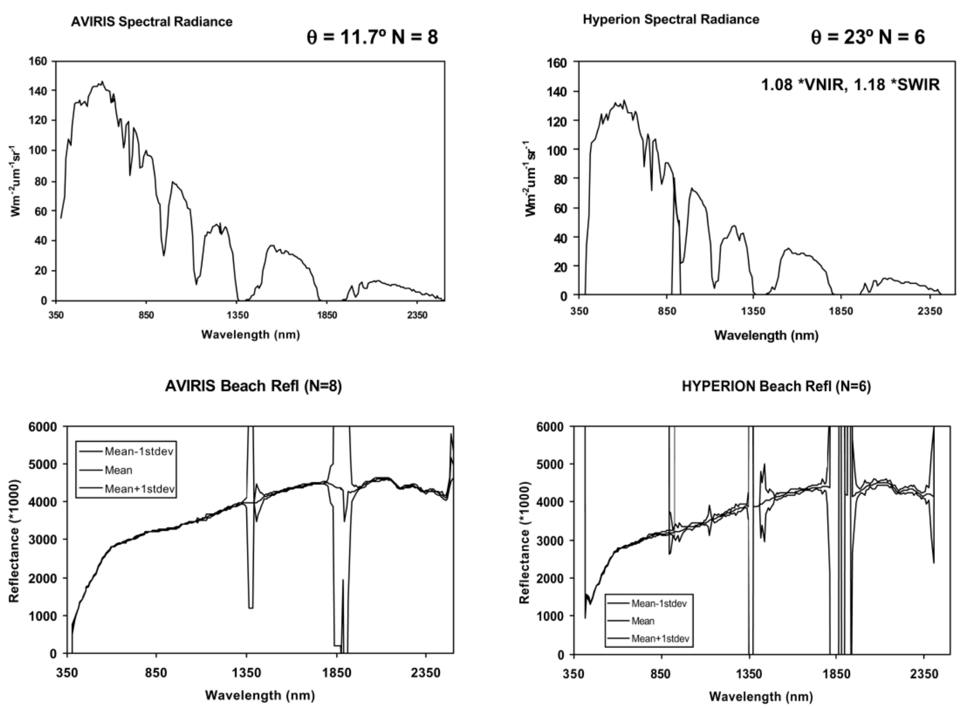

(a) (b)

Fig. 2. Radiance and reflectance spectra of the west beach ground calibration target. (a) AVIRIS spectra. (b) Hyperion. Plots show the mean ± one standard deviation based on eight (AVIRIS) or six (Hyperion) spectra. A lower number of targets is used for Hyperion because it has a coarser spatial resolution.

selected accounting for all but 24 spectra out of the 92. Analysis of the remaining members of the library demonstrated that most required a third endmember and were, thus, not suitable candidates. For oak, five spectra were selected that accounted for all but 19 out of 178 spectra in the oak-dominated library. The top choice in this case was evf86.19, which accounted for 75.3% of the library.

The extent of confusion between species is also illustrated in Table I. For example, if we consider the chamise-dominated spectrum, evf57.14, this spectrum is relatively distinct from oak, modeling only 6.7% of oak library but is confused with *Ceanothus*- and manzanita-dominated spectra, modeling 37.8% and 76.9% of the members of these libraries. The oak spectra, on the other hand, are rarely confused with chamise and never confused with manzanita, but often confused with *Ceanothus*.

A total of 27 two-endmember models were selected using the process described above. Models included five soils, five NPV, four chamise, five *Ceanothus*, three manazanita, and five

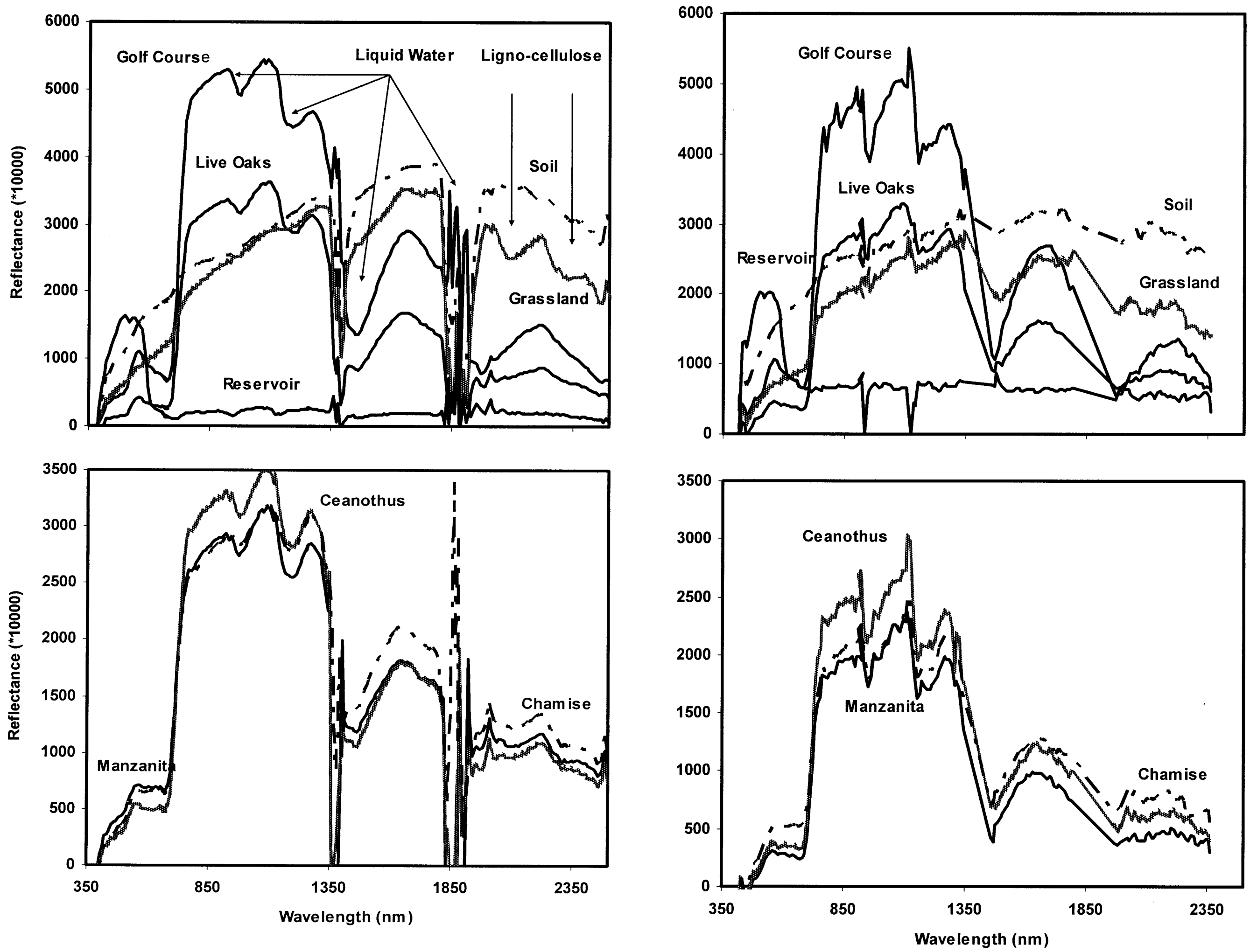

Fig. 3. Reflectance spectra for eight common materials. (a) AVIRIS spectra. (b) Hyperion spectra. The upper frames show five common materials, including a reservoir, golf course, live oaks, soil, and grassland. The lower frames show three chaparral dominants: manzanita, *Ceanothus*, and chamise. The arrows point to important chemical absorption features.

oak spectra. For three-endmember models, one endmember was selected from each of the six classes that accounted for the largest area mapped. These spectra were used to develop sets of three-endmember models corresponding to soil-NPV-shade, Soil-GV-shade, and NPV-GV-shade. A total of 20 three-endmember models were applied to the image.

AVIRIS spectra selected using this process were translated to equivalent Hyperion spectra using cubic spline interpolation and the AVIRIS and Hyperion band centers. The same sets of two- and three-endmember models developed for AVIRIS were applied to Hyperion.

IV. Results/Discussion

A. Reflectance Retrieval

Surface reflectances retrieved from Hyperion and AVIRIS using ACORN are comparable (Figs. 2 and 3). Radiance measured from AVIRIS (upper left) and Hyperion (right) exhibit a similar shape, differing primarily because of the larger solar zenith angle for Hyperion (23°) relative to AVIRIS (12°). Importantly, the postlaunch radiance corrections used here are general corrections developed earlier in the life of Hyperion, suggesting that the sensor is radiometrically stable. Higher noise levels in Hyperion result in a higher standard deviation shown in the spectra. Based on NEdL, Hyperion appears to have a signal to noise approximately five times worse than AVIRIS; NEdL for AVIRIS was estimated as 0.021 $Wm^{-2}\mu msr^{-1}$, with Hyperion equal to 0.107 $Wm^{-2}\mu msr^{-1}$, at 1851 nm.

Hyperion reflectance was compared to AVIRIS for a selection of dominant vegetation types (Fig. 3). The general shape of retrievals is similar, although a higher solar zenith for Hyperion results in decreased reflectance in vegetation while poorer instrumental performance results in a higher standard deviation. Hyperion has the ability to resolve most of the major chemical features of vegetation (water, chlorophyll, ligno-cellulose bands) and showed the same general trends in brightness, with highest NIR reflectance found in golf courses. The ability of Hyperion to resolve ligno-cellulose bands, and thus distinguish NPV from soils, is particularly significant for fire danger assessment.

To evaluate the potential of Hyperion for species-level mapping, spectra of chamise, manzanita, and *Ceanothus* extracted

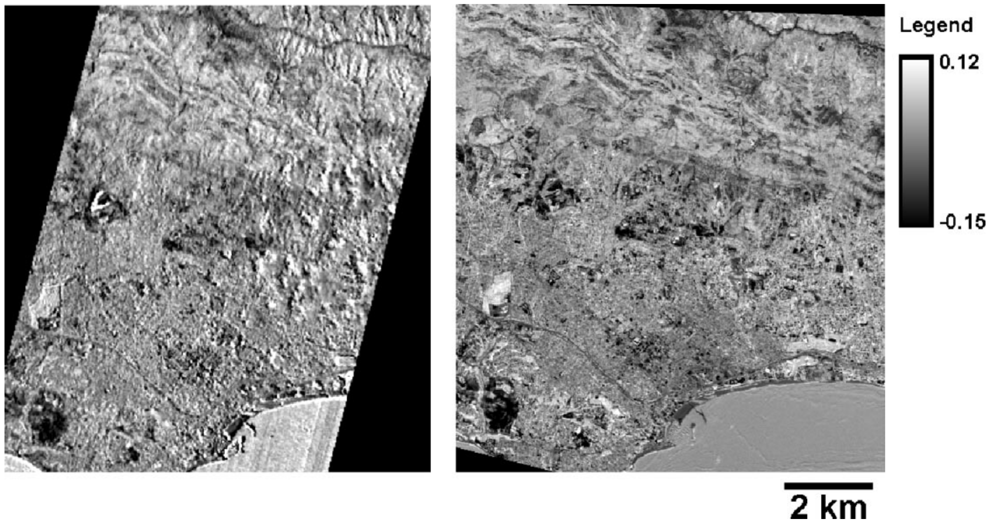

(a) (b)

Fig. 4. Images showing NDWI for (a) Hyperion and (b) AVIRIS. Artifacts in Hyperion are evident as down-track striping, sharpened edges, and high NDWI values on the right side of the image.

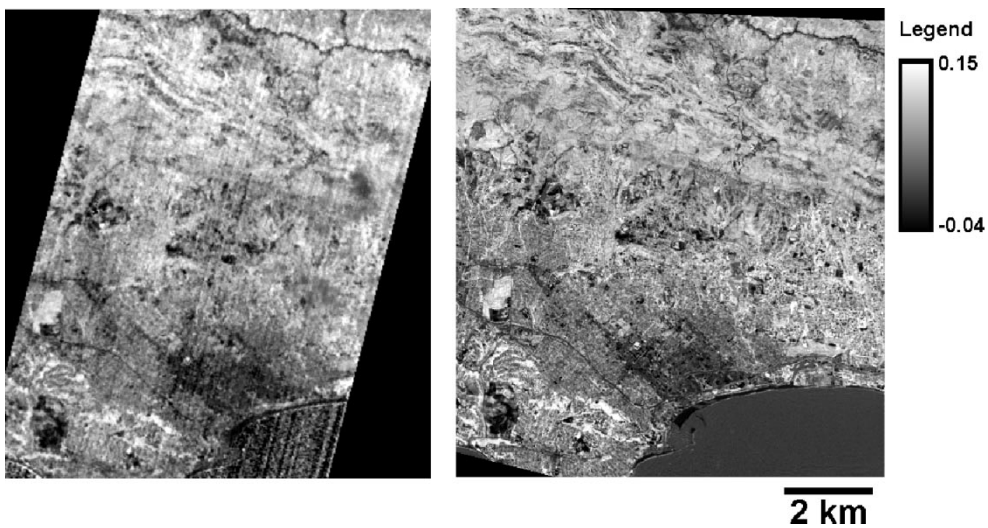

(a) (b)

Fig. 5. Images showing mNDWI for (a) Hyperion and (b) AVIRIS. Down-track striping is enhanced in Hyperion, but edge effects and spectral smile are minimized.

from the reference polygons for both were compared for both sensors (Fig. 3, lower left and right). Subtle differences in the spectra are evident with lower visible reflectance, higher NIR reflectance, and the lowest SWIR shown for *Ceanothus*. Chamise and manzanita have comparable visible reflectance and NIR, but chamise has higher reflectance in the SWIR. The same general trends are observed in Hyperion, although the overall reflectance is lower because of the larger zenith. Hyperion spectra show considerably higher variance than AVIRIS spectra, especially in strong liquid water bands at 980 nm and in the SWIR.

B. Fuel Moisture/Live Biomass

All Hyperion measures dependent upon the 980-nm liquid water band performed poorly due to very low signal in this wavelength region [27]. Images for the WI and EWT980 are not shown due to space limitations. NDWI performance was generally good (Fig. 4). In this figure, NDWI is scaled from -0.15 to 0.12 (dark to bright). The general patterns measured by AVIRIS are captured by Hyperion. For example, senesced areas have low NDWI in both scenes; dense vegetation has high NDWI in both scenes as well. However, Hyperion is subject to a large number of spatial artifacts that reduce its effectiveness. For example, vertical striping is evident, resulting from the design of the instrument in which each cross-track element corresponds to a different spectrometer. High NDWI values on the right side of a Hyperion image are possibly due to cross-track wavelength shifts, commonly referred to as spectral smile. Misalignment between the VNIR and SWIR focal planes results in enhanced edges when bands from the two different portions of the spectrum are ratioed. For a detailed discussion of Hyperion artifacts and their origins, see [27].

As anticipated, mNDWI showed even greater correspondence between Hyperion and AVIRIS (Fig. 5). Low and high values of mNDWI from the two sensors are similar. Although vertical striping is still present in Hyperion, enhanced edges and the effects of spectral smile do not appear to be as severe. EWT1200

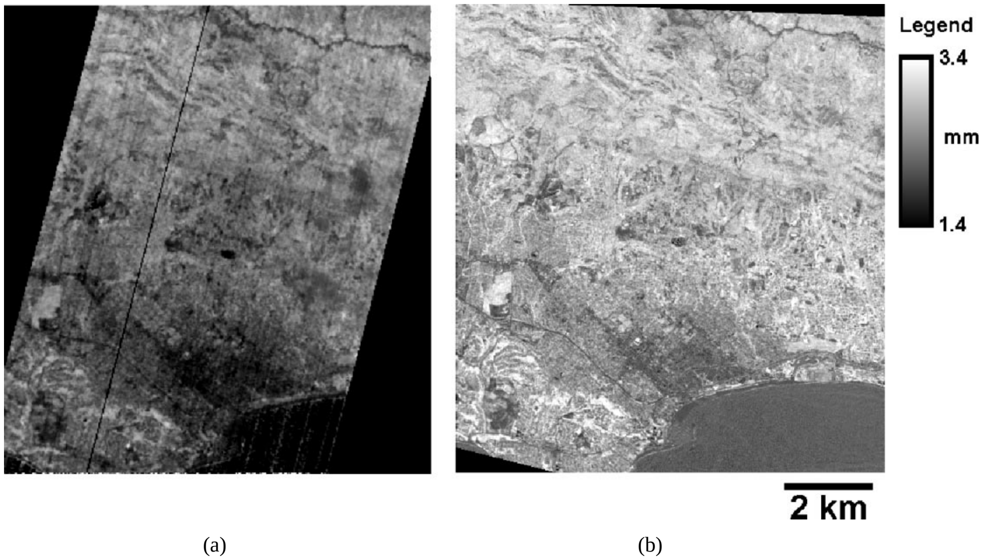

Fig. 6. Image showing EWT1200 for (a) Hyperion and (b) AVIRIS. Down-track striping and the black line on the left of the Hyperion image are artifacts.

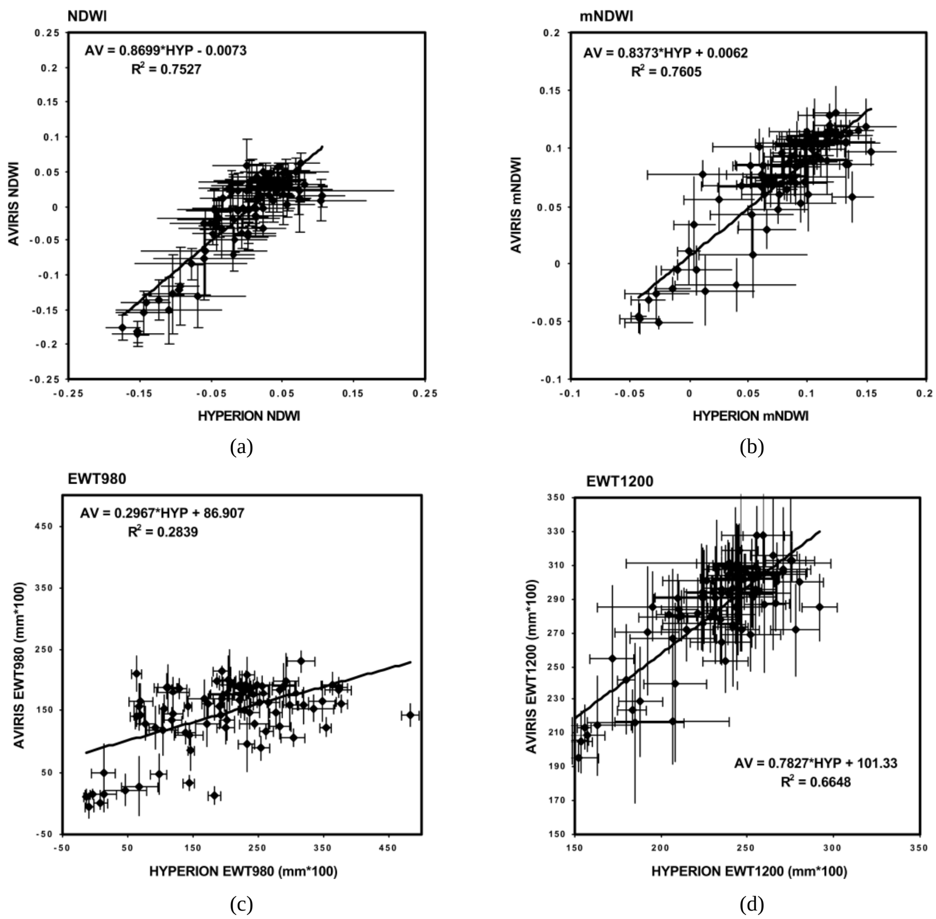

Fig. 7. Scatterplots showing various moisture measures from Hyperion (x) and AVIRIS (y). The central point is the mean derived from reference polygons, and error bars equal one standard deviation. Plots show (a) NDWI, (b) mNDWI, (c) EWT980, and (d) EWT1200.

showed similar performance to the mNDWI (Fig. 6). However, in this case there was a significant bias between the two sensors, resulting in significant brightness differences between the images, especially for areas where EWT1200 was low.

More quantitative comparisons were made using scatterplots, plotting AVIRIS along the y axis and Hyperion along the x (Fig. 7). Error bars on all points represent ± 1 standard deviation. The data points plotted represent mean and standard deviations determined from the reference polygons. The highest correlation between AVIRIS and Hyperion was observed for mNDWI, followed by NDWI, which had r^2 values 0.76 and 0.75, respectively. Slopes between the two measures departed from a 1 : 1 relationship, with Hyperion consistently showing higher values in both cases. Error bars were generally higher for Hyperion than

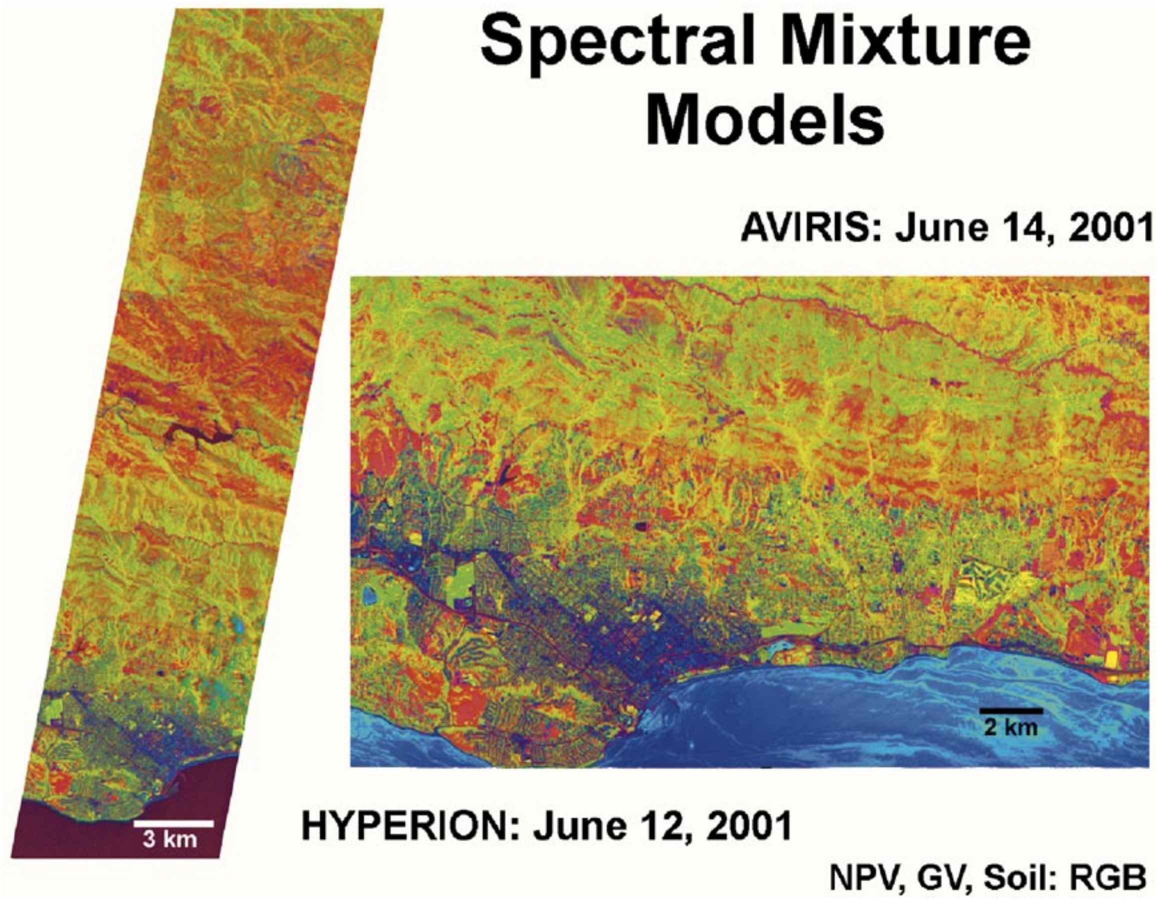

Fig. 8. False color composite showing fraction images for NPV (red), GV (green), and soil (blue).

AVIRIS, consistent with image artifacts and the lower SNR for Hyperion. In both cases, the intercept was near zero. EWT1200 showed a similarly high correlation between the two sensors, with an r^2 of 0.66. The slope departed significantly from a 1 : 1 relationship. Unlike the NDWI and mNDWI, the intercept departed significantly from zero, equal to 1.01 mm. The relationship between EWT980 for the two sensors was poor, with an r^2 of 0.28. Hyperion showed a much larger range of EWT980 values than AVIRIS, due to low SNR for Hyperion in this spectral region [27]. Poor performance of EWT980 derived from Hyperion data, while not surprising, is unfortunate because the 980-nm band is the most commonly used wavelength and is generally superior for moisture assessment due to the proximity of the 1200-nm band to the primary water vapor band centered at 1500 nm.

C. Fuel Condition

Hyperion's ability to map fuel condition using SMA was good (Fig. 8). In this figure, areas mapped as red (NPV) are considered to have the highest fire danger because of an abundance of senesced plant material. Areas with high GV fractions are considered to have lower danger because of the presence of large amounts of live leaf material with its associated moisture. Areas with high soil fractions (blue), would be considered low risk areas due to a lack of combustable fuels. The highest GV fractions are in golf courses and parks with moderate levels in more mesic sites dominated by *C. spinosus* and *Q. agrifolia*. The lowest GV fractions were found primarily in senesced grasslands, which were mapped as almost pure NPV.

Similarities between Hyperion and AVIRIS for broad-based spectral measures are not surprising. SMA, because it utilizes the entire spectrum, not just a few wavelengths, will be less sensitive to sensor noise in individual bands. Unless the errors are systematic, noise in individual bands will tend to cancel out when fit is assessed across all wavelengths. Although Hyperion has a coarser spatial resolution of 30 m, the larger areal coverage is a major advantage relative to an airborne sensor.

More quantitative comparisons were made using scatterplots of AVIRIS (y) modeled fraction against Hyperion (x) modeled fraction (Fig. 9). NPV measured by the two sensors was nearly identical, with a slope near one and intercept near zero (0.03) and a high r^2 (0.75). This is a very encouraging result, because it is difficult to distinguish NPV from soil using broadband sensors, and NPV is a critical component of fuel. Higher scatter for Hyperion, caused by lower SNR, is evident in the larger error bars. A similar relationship was observed for soils (lower left), which had a slope near one, an r^2 of 0.77, and an intercepted that departed only slightly off of zero. The most significant difference between the sensors was observed for the GV and shade fractions. GV showed the highest r^2 (0.83), but had a slope significantly greater than one. The most likely explanation is the difference in solar zenith. Hyperion, which was acquired at a solar zenith of 23°, would be expected to have a much higher

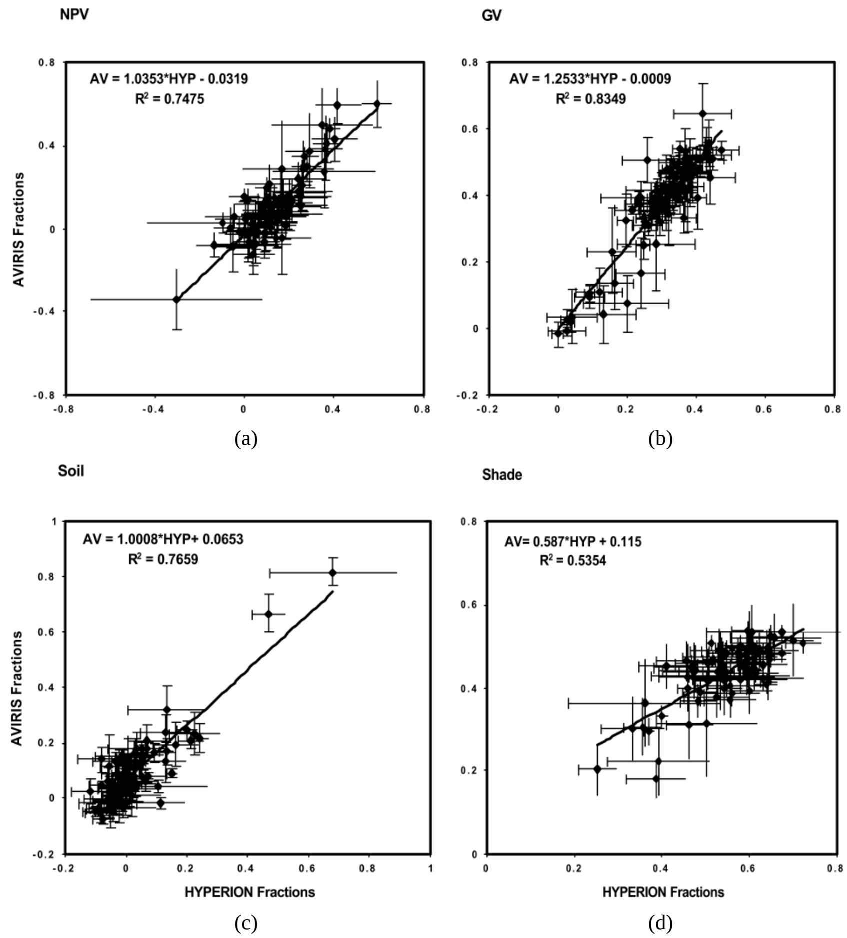

Fig. 9. Scatterplots showing spectral fractions from Hyperion (x) and AVIRIS (y). The central point is the mean derived from reference polygons, and error bars equal one standard deviation. Plots show (a) NPV, (b) GV, (c) soil, and (d) shade.

shade fraction than AVIRIS, in which the solar zenith was only 12°. Because the fractions are constrained to sum to unity, a high shade fraction in Hyperion translates to lower fractions for the other endmembers. The differences are most significant for live vegetation because these surfaces have greater vertical expression and, thus, cast shadows, whereas shadowing is only minor in senesced grasslands and bare soil. The lowest correlation was found for shade (0.54), most likely because this fraction includes a mixture of cover types that cast shadows (live vegetation) and cover types that do not (senesced grasslands and bare soil). A plot of shade restricted to bare soil and grasslands would be expected to be closer to a 1 : 1 line with a higher r^2.

1) Fuel Type Maps: Vegetation dominance was mapped for Hyperion and AVIRIS for six dominant classes: soil (red), senesced grass (yellow), chamise (orange), *Ceanothus* (blue), manzanita (cyan), and oak (green); see Fig. 10. In general, the AVIRIS map for dominance is consistent with expected locations, showing manzanita at higher elevations where it occurs, oaks in valleys, *Ceanothus* on the lower elevation slopes, and chamise at high elevations along the spine of Santa Ynez Range. Soils and grasslands appear to be mapped correctly. Visual comparison between AVIRIS and Hyperion indicates that soils, grasslands, and chamise are mapped in similar locations by the two sensors. However, significant differences are evident as well: larger areas are mapped as *Ceanothus*-dominated by AVIRIS and mapped as oak by Hyperion. More subtle differences are also evident, in which many areas mapped as chamise-dominated by AVIRIS are mapped as *Ceanothus*-dominated by Hyperion.

Performance of the two sensors was evaluated by comparison to the reference polygons measured in the field. Standard measures of accuracy include overall accuracy (correct/total), producer's accuracy (correct/reference), user's accuracy (correct/mapped), and Kappa [32]. When comparing two classifiers, an accepted procedure is to calculate Kappa variance [33], [34] and compare Z values for each classified map.

AVIRIS accuracy was assessed using 91 polygons, 79 of which were located in the overlap zone between the two sensors and were sufficiently large enough to constitute at least six pixels at 30-m resolution (Table II). Overall accuracy of AVIRIS was found to be 79.1%, below a desirable level of 85% with a kappa of 0.722. Producer's accuracies for each class ranged from 100% for 15 grassland-dominated sites, to a low of 28.6% for manzanita-dominated sites (Table II). Most classes were mapped with individual accuracies between 75% and 85.7%. With the exception of manzanita, all classes met a minimum 70% accuracy. According to the error matrix, the greatest source of confusion was between *Ceanothus* and oaks, in which six *Ceanothus*-dominated polygons were mapped as oak-dominated and where two oak-dominated polygons were mapped as *Ceanothus*-dominated. A majority of the manzanita-dominated sites were misidentified as *Ceanothus*,

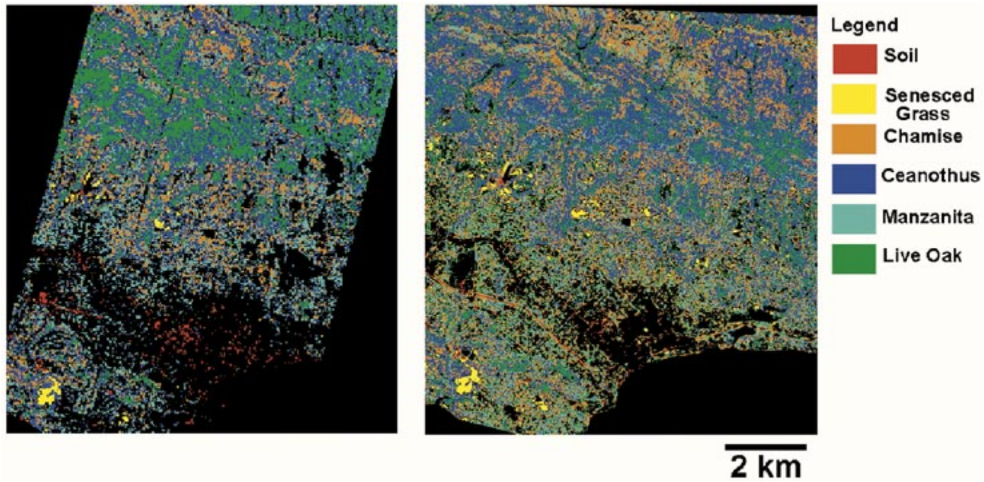

Fig. 10. Images showing vegetation dominants mapped using MESMA. Six classes are shown including soil (red), senesced grass (yellow), chamise (orange), *Ceanothus* (blue), manzanita (cyan), and oak (green).

TABLE II
ERROR MATRIX FOR AVIRIS. COLUMN TOTALS ARE FOR REFERENCE DATA, ROWS IMAGE CLASSES. INCLUDES SEVEN CLASSES: SOIL, GRASS, CHAMISE, CEANOTHUS (CEANO), MANZANITA (MANZAN), OAK, UNCLASSIFIED (UNCL), PRODUCER'S (PROD), USER'S, AND OVERALL ACCURACIES (ACCUR)

	soil	grass	chamise	ceano	manzan	oak	uncl	Totals	Users
soil	**6**							6	**1**
grass		**15**						15	**1**
chamise			**12**	1				13	**0.923**
ceano			1	**31**	5	2		39	**0.795**
manzan					**2**			2	**1**
oak				6		**6**		12	**0.5**
uncl	1		**3**					4	
Totals	7	15	16	38	7	8			**91**
Prod	**0.857**	**1**	**0.75**	**0.816**	**0.286**	**0.75**			72
								Accur	**0.791**
	Kappa	**0.722**							

although in most of the cases, the second most abundant class in the polygon was manzanita. User's accuracies ranged from 50% for oak to 100% for soils, grasslands and manzanita with 92.3% for chamise and 79.5% for *Ceanothus*. Low user's accuracies for oak- and *Ceanothus*-dominated polygons suggests that these two classes are overmapped.

Confusion between oak and *Ceanothus* was anticipated based on the process used to select reference endmembers (Table I). During library development, the two species most often confused were *Ceanothus* and oaks, with some confusion being unavoidable. Poor performance for manzanita was not anticipated based on the spectral library. During this analysis, manzanita proved to be highly distinct from all classes except chamise. More detailed analysis of the two- and three-endmember models identified the source of the error. In the case of two-endmember models, manzanita was selected as the correct model in almost all cases. However, the fit was poor (high rms), primarily because the library lacked spectra for the rock outcrops commonly found in association with the manzanita. When expanded to include a third endmember, the GV model switched to *Ceanothus* and soil, and the rms dropped significantly. In essence, the wrong vegetation when combined with the wrong soil fit better than the right vegetation without soil included in the model. Inclusion of the correct rock spectrum in the library would be expected to eliminate this source of error, but because spectra were extracted from the image, this was not possible because the rocks are only pure at subpixel scales.

Hyperion performance was considerably worse than AVIRIS with an overall accuracy of 0.506 and kappa of 0.318 based on 85 points (several used for AVIRIS were off the scene) (Table III). Producer's accuracies ranged from a low of only 12.75% for manzanita to a high of 100% for soils (only two sites were used, however). Most producer's accuracies were unacceptably low ranging from 33.3% (chamise) to 57.1% for oak. User's accuracies were better, with three categories (soils, grass, and chamise) mapped at 100%. In most cases, greater confusion with Hyperion could be predicted from the library and AVIRIS analysis. Confusion between classes experienced with AVIRIS was exacerbated by Hyperion, including an increased confusion between oaks, *Ceanothus*, and manzanita. Oaks were substantially overmapped at the expense of *Ceanothus*, while many reference polygons of chamise or manzanita were mapped as *Ceanothus*.

Performance of Hyperion and AVIRIS was compared using 79 overlapping reference polygons with at least six pixels in each polygon. Based on this more limited set of reference polygons, AVIRIS and Hyperion overall accuracy dropped slightly, equal to 77.2% and 49.4%, respectively. Kappa also

TABLE III
ERROR MATRIX FOR HYPERION. COLUMN TOTALS ARE FOR REFERENCE DATA, ROWS IMAGE CLASSES. INCLUDES SEVEN CLASSES: SOIL, GRASS, CHAMISE, CEANOTHUS (CEANO), MANZANITA (MANZAN), OAK, UNCLASSIFIED (UNCL), PRODUCER'S (PROD), USER'S, AND OVERALL ACCURACIES (ACCUR)

	soil	grass	chamise	ceano	manzan	oak	uncl	Totals	Users
soil	**2**							2	**1**
grass		**9**						9	**1**
chamise			**6**					6	**1**
ceano		1	9	**21**	7	3		41	**0.512**
manzan			1		**1**			2	**0.5**
oak			2	17		**4**		23	**0.174**
uncl		1		1				2	
Totals	2	11	18	39	8	7	0		**85**
Prod	**1**	**0.818**	**0.333**	**0.538**	**0.125**	**0.571**			43
								Accur	**0.506**
	Kappa	**0.318**							

decreased, equaling 0.675 for AVIRIS and 0.289 for Hyperion. Kappa variance was calculated as 0.004 495 for AVIRIS and 0.007 479. Based on a calculation of the Z statistic from Kappa and Kappa variance, AVIRIS outperformed Hyperion at above the 0.95 confidence level ($Z = 3.528$). While Hyperion performance was disappointing, the ability of Hyperion to distinguish soils from senesced grasslands, which is commonly infeasible with a broadband sensor, is very important for fire danger assessment. Chamise, a very important chaparral fuel, was also well mapped by Hyperion, with a high user's accuracy. Lower accuracies for Hyperion likely result from a number of factors including a lower SNR, coarser spatial resolution, spatial artifacts, and a higher solar zenith. For example, many of the spectral differences between chaparral species are subtle (Fig. 3). Furthermore, chaparral is typically patchy, with fairly small uniform patch size. A decrease in SNR, lower overall reflectance, and coarser spatial resolution would be expected to reduce separability of these classes. Correction of spatial artifacts, such as vertical striping and spectral smile, would improve Hyperion performance.

V. CONCLUSION

In this paper, we evaluated the performance of Hyperion relative to AVIRIS for fire danger assessment. We focused on the Santa Barbara area, a region that has experienced a number of recent catastrophic fires. We compared reflectance, measures of fuel moisture/live biomass, fuel condition, and fuel type derived from spatially overlapping Hyperion and AVIRIS datasets acquired in early June 2001.

Postlaunch radiometric calibration of Hyperion is remarkably good, producing radiance values that are similar to AVIRIS and resulting in high-quality retrievals of surface reflectance. Radiometric stability appears to be good, which is a fundamental requirement for monitoring surface change. The SNR of Hyperion appears to be, at best, 20% of AVIRIS based on the NEdL. All measures of canopy moisture based on the 980-nm liquid water band proved to be ineffective for measurement by Hyperion. However, measures based on the 1200-nm band, such as EWT1200, NDWI, or mNDWI, provided a good match to AVIRIS, suggesting that Hyperion can map canopy moisture for across a wide range of vegetation types. Measures of fuel condition, derived using SMA, were essentially the same between the two sensors, showing a 1 : 1 correspondence for soil and NPV, but differing for shade and GV due to differences in solar zenith. The ability of Hyperion to distinguish NPV from soils is particularly valuable, because NPV is an important component of fire danger assessment that cannot be distinguished from soils using broadband systems except under limited conditions (i.e., grasses are confused with many, but not all soils).

Vegetation types were mapped using MESMA. While neither sensor exceeded 85% accuracy, AVIRIS came close to this requirement and produced a map significantly more accurate than Hyperion. However, Hyperion was capable of mapping three critical land-cover classes at high accuracy that are of importance to fire danger: bare soil, senesced grasslands, and chamise.

Although a spaceborne imaging spectrometer, such as Hyperion, does not have the instrumental performance of AVIRIS, it has several advantages. First, the ability to image portions of the globe that cannot be visited by an aircraft is nontrivial. Although we do not take advantage of it here, a 16-day repeat cycle offers the potential of mapping seasonal changes in fuel properties that cannot be readily done from an airborne platform. For example, at least three other Hyperion datasets have been acquired over Santa Barbara, including data from March, May, and November 2001.

ACKNOWLEDGMENT

The authors wish to acknowledge the Jet Propulsion Laboratory, which loaned the ASD full-range instrument used in this research and supplied radiometrically calibrated AVIRIS data. Thanks also to G. Asner and one anonymous reviewer for helpful comments used to revise this paper.

REFERENCES

[1] M. A. Cochrane, M. A. , A. Alencar, A. , M. D. Schulze, C. M. Souza, D. C. Nepstad, P. Lefebvre, and E. A. Davison, "Positive feedbacks in the fire dynamics of closed canopy tropical forest," *Science*, vol. 284, pp. 1832–1835, 1999.

[2] W. M. Hao and M. H. Liu, "Spatial and temporal distribution of tropical biomass burning," *Global Biogeochem. Cycles*, vol. 8, no. 4, pp. 495–503, 1994.

[3] E. S. Kasischke, N. H. French, P. Harrel, N. L. Christensen, S. L. Ustin, and D. A. Barry, "Monitoring of wildfires in boreal forests using large area AVHRR NDVI composite data," *Remote Sens. Environ.*, vol. 44, pp. 61–72, 1993.

[4] S. J. Pyne, P. L. Andrews, and R. D. Laven, *Introduction to Wildland Fire*, 2nd ed. New York: Wiley, 1996.
[5] S. R. Yool, D. W. Eckhardt, D. W. , and M. J. Cosentino, "Describing the brushfire hazard in southern California," *Anal. Assoc. Amer. Geograph.*, vol. 75, pp. 431–442, 1985.
[6] California State Board of Forestry, "California fire plan: A Framework for minimizing costs and losses from wildland fires," California State Board of Forestry, Sacramento, CA, 1996.
[7] K. W. H. Radtke, A. Arndt, R. H. Wakimoto, and R. H. , "Fire history of the Santa Monica Mountains,", USDA FS Tech. Rep. PSW-58, Dynamics and Management of Mediterranean-type Ecosystems, C. E. Conrad and W. C. Oechel, Eds., 1982.
[8] S. C. Barro and S. G. Conard, "Fire effects on California chaparral systems: An overview," *Environ. Int.*, vol. 17, pp. 135–149, 1991.
[9] H. E. Anderson, "Aids to determining fuel models for estimating fire behavior," USDA Forest Service, Intermountain Forest and Range Experiment Station, INT-122, 1982.
[10] C. Philpot, "Vegetative features as determinants of fire frequency and intensity," in *Proc. Symp. on Environmental Consequences of Fire and Fuel Management in Meditteranean Ecosystems*, Palo Alto, CA, 1977.
[11] D. Gomes, O. L. Graham, E. H. Marshall, and A. J. Schmidt, "Sifting through the ashes, lessons learned from the painted cave fire," Univ. of California, Santa Barbara, South Coast Historical Series, Graduate Program in Public Historical Studies, 1993.
[12] J. B. Adams, M. O. Smith, M. O. , and A. R. Gillespie, "Imaging spectroscopy: Interpretation based on spectral mixture analysis," in *Remote Geochemical Analysis: Elemental and Mineralogical Composition*, C. M. Pieters and P. Englert, Eds, NY: Cambridge Univ. Press, 1993, vol. 7, pp. 145–166.
[13] D. A. Roberts, M. Gardner, R. Church, S. Ustin, G. Scheer, and R. O. Green, "Mapping chaparral in the Santa Monica mountains using multiple endmember spectral mixture models," *Remote Sens. Environ.*, vol. 65, pp. 267–279, 1998.
[14] R. E. Burgan and M. B. Shasby, "Mapping broad-area fire potential from digital fuel, terrain and weather data," *J. Forestry*, vol. 8, pp. 228–231, 1984.
[15] E. Chuvieco, E. , and R. G. Congalton, "Application of remote sensing and geographic information systems to forest fire hazard mapping," *Remote Sens. Environ*, vol. 29, pp. 147–159, 1989.
[16] E. Chuvieco, J. Salas, and J. , "Mapping the spatial distribution of forest fire danger using gis," *Int. J. GIS*, vol. 10, no. 3, pp. 333–345, 1996.
[17] L. S. Bradshaw, J. E. Deeming, R. E. Burgan, J. D. Cohen, and D. Jack, "The 1978 national fire-danger rating system: Technical documentation," USDA Forest Service Intermountain Forest and Range Experiment Station, Gen. Tech. Rep. INT-169, 1978.
[18] D. A. Roberts, P. E. Dennison, M. Morais, M. E. Gardner, J. Regelbrugge, S. L. Ustin, and S. L. , "Mapping wildfire fuels using imaging spectrometry along the wildland urban interface," in *Proc. Joint Fire Science Conf. Workshop*, vol. 1, Boise, ID, June 17–19, 1999, pp. 212–223.
[19] P. E. Dennison, D. A. Roberts, and J. C. Regelbrugge, "Characterizing chaparral fuels using combined hyperspectral and synthetic aperture radar data," in *Proc. 9th AVIRIS Earth Science Workshop*, vol. 6. Pasadena, CA, Feb. 23–25, 2000, pp. 119–124.
[20] R. O. Green, J. E. Conel, and D. A. Roberts, "Estimation of aerosol optical depth and calculation of apparent surface reflectance from radiance measured by the Airborne Visible-Infrared Imaging Spectrometer (AVIRIS) using MODTRAN2," in *Proc. SPIE Imaging Spectrometry of the Terrestrial Environment*, vol. 1937, 1993, pp. 2–5.
[21] D. A. Roberts, R. O. Green, R. O. , and J. B. Adams, "Temporal and spatial patterns in vegetation and atmospheric properties from AVIRIS," *Remote Sens. Environ*, vol. 62, pp. 223–240, 1997.
[22] B.-C. Gao, "NDWI-A normalized difference water index for remote sensing of vegetation liquid water from space," *Remote Sens. Environ.*, vol. 58, pp. 257–266, 1996.
[23] J. Penuelas, I. Filella, C. Biel, L. Serrano, and R. Save, "The reflectance at the 950–970 nm region as an indicator of plant water status," *Int. J. Remote Sens.*, vol. 14, pp. 1887–1905, 1993.
[24] D. A. Roberts, K. J. Brown, R. Green, R. , S. Ustin, and T. Hinckley, "Investigating the relationship between liquid water and leaf area in clonal populus," in *Proc. 7th AVIRIS Earth Science Workshop*. Pasadena, CA, 1998, JPL 97–21, pp. 335–344.
[25] S. L. Ustin, S. L. , D. A. Roberts, J. Pinzon, S. Jacquemoud, M. Gardner, G. Scheer, C. M. Castaneda, and A. Palacios, "Estimating canopy water content of chaparral shrubs using optical methods," *Remote Sens. Environ.*, vol. 65, pp. 280–291, 1998.
[26] L. Serrano, S. L. Ustin, D. A. Roberts, J. A. Gamon, and J. Penuelas, "Deriving water content of chaparral vegetation from AVIRIS data," *Remote Sens. Environ.*, vol. 74, pp. 570–581, 2000.
[27] S. Ungar, J. Pearlman, J. Mendenhall, and D. Reuter, "Overview of the Earth Observing One (EO-1) Mission," *IEEE Trans. Geosci. Remote Sens.*, vol. 41, pp. 1149–1159, June 2003.
[28] R. O. Green *et al.*, "Imaging spectroscopy and the Airborne Visible Infrared Imaging Spectrometer (AVIRIS)," *Remote Sens. Environ.*, vol. 65, no. 3, pp. 227–248, 1998.
[29] R. O. Green, B. E. Pavri, and T. G. Chrien, "On-orbit radiometric and spectral calibrat ion characteristics of EO-1 Hyperion derived with an underflight of AVIRIS and *in situ* measurements at Salar de Arizaro, Argentina," *IEEE Trans. Geosci. Remote Sensing*, vol. 41, pp. 1194–1203, June 2003.
[30] R. N. Clark, G. Swayze, K. Heidebrecht, A. F. H. Goetz, and R. O. Green, "Comparison of methods for calibrating AVIRIS data to ground reflectance," *Summaries of the 4th Annu. JPL Airborne Geoscience Workshop*, vol. 1, Oct. 1993.
[31] D. A. Roberts, M. Gardner, R. Church, S. L. Ustin, and R. O. Green, "Optimum strategies for mapping vegetation using multiple endmember spectral mixture models," in *Proc. SPIE Conf. Imaging Spectrometry III*, San Diego, CA, 1997.
[32] R. Congalton, "A review of assessment the accuracy of classifications of remotely sensed data," *Remote Sens. Environ.*, vol. 37, no. 35-46, 1991.
[33] R. Congalton and R. A. Mead, "A quantitative method to test for consistency and correctness in photointerpretatin," *Photogram. Eng. Remote Sens.*, vol. 49, no. 1, pp. 69–74, 1983.
[34] W. D. Hudson and C. W. Ramm, "Correct formulation of the kappa coefficient of agreement," *Photogramm. Eng. Remote Sens.*, vol. 53, no. 4, pp. 421–422.

Dar A. Roberts (M'94) was born in Torrance, CA, in 1960. He received the B.A. degree (double major in geology and environmental biology) from the University of California, Santa Barbara, in 1981, the M.A. degree in applied earth sciences from Stanford University, Stanford, CA, in 1986, and the Ph.D. degree in geological sciences from the University of Washington, Seattle, in 1991.

He is currently an Associate Professor in the Department of Geography, University of California, Santa Barbara, where he started in January 1994. His primary research interests are in remote sensing of vegetation, spectroscopy, hyperspectral remote sensing, land-cover mapping, change detection, sensor fusion, and algorithm development, primarily for spectral mixture analysis. He has worked extensively with airborne hyperspectral data since 1985, synthetic aperture radar since 1996, and most recently hyperspectral thermal imaging spectrometry data. He teaches an advanced graduate level course in microwave and optical remote sensing.

Dr. Roberts is a member of the Ecological Society of America, the Association of American Geographers, and the American Society of Photogrammetry.

Philip E. Dennison (S'98) received the B.S. degree in geography from the Pennsylvania State University, University Park, in 1997, and the M.A. degree in geography from the University of California, Santa Barbara, in 1999. He is currently pursuing the Ph.D. degree in geography from the University of California, Santa Barbara.

His research interests include remote sensing of vegetation phenology, hyperspectral and synthetic aperture radar remote sensing of vegetation, remote sensing of fuel moisture for fire hazard prediction, and fire behavior modeling.

Mr. Dennison is the recipient of a National Aeronautics and Space Administration Earth Systems Science Fellowship.

Margaret E. Gardner was born in Knoxville, TN, in 1971. She received the B.S. degree in geography from James Madison University, Harrisonburg, VA, and the M.A. degree from the University of California, Santa Barbara, in 1993.

She is currently a Researcher with the University of California, Santa Barbara, with a focus in hyperspectral remote sensing applications. She was a Remote Sensing Analyst and Project Manager for Pacific Meridian Resources, Emeryville, CA from 1998 to 1999.

Yasha Hetzel received the B.S. degree in geography from the University of California, Santa Barbara (USCB), in 2001.

He has supported remote sensing field research in Southern California, Hawaii, and South Africa for UCSB.

Susan L. Ustin (M'90) received the B.S. and M.S. degrees in biology from the California State University, Hayward, and the Ph.D. degree in botany in the area of plant physiological ecology from the University of California, Davis (UC Davis).

She is currently a Professor in the Department of Land, Air, and Water Resources, UC Davis. Since 1983, her research has focused on the use of remote sensing instruments to measure ecological properties and processes. In particular, she has been active in the development of imaging spectrometery from airborne and spaceborne platforms for measuring ecosystem properties. Her research has focused on developing and testing methods for retrieving environmental information from remote sensing imagery at spatial scales from microscopic to regional and encompasses both theoretical and applied research. She has studied many different ecological communities and farmlands in the United States and abroad. She is Director of the UC Davis California Space Institute Center of Excellence and the Center for Spatial Technologies and Remote Sensing (CSTARS), and is Director of the Department of Energy's Western Center for Global Environmental Change (WESTGEC), Davis, CA.

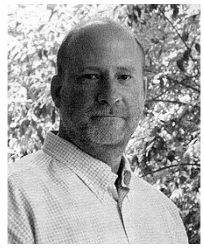

Christopher T. Lee (M'02) was born in Los Angeles, CA, in 1954. He received the B.S. degree from Northern Arizona University (NAU), Flagstaff, in 1978, the M.A. degree from California State University, Fullerton, in 1982, and the Ph.D. degree from the University of Arizona, Tucson, in 1990, all in geography.

He is currently a Professor in the Department of Geography, California State University, Long Beach He has almost 20 years of university-level teaching experience in remote sensing and physical geography. After teaching at NAU and the University of Arizona from 1984 to 1990, he was an Assistant, Associate, and Full Professor at California State University, Dominguez Hills, from 1991 to 2000. His primary research interests are in remote sensing of arid lands and in geospatial workforce development. He was a Fulbright Scholar to Egypt in 1995–1996 and was a Visiting Senior Scientist assigned to the Applications Division, NASA Headquarters, Washington, DC., in 1999.

Dr. Lee is a member of the Association of American Geographers, the Royal Geographical Society, the American Society of Photogrammetry, and the Explorers Club.